Design of Isoform-Selective Enzyme Inhibitors by Exploring Pocket Size According to the Lock-and-Key Principle

*Virginija Dudutienė[a], Asta Zubrienė[a], Visvaldas Kairys[b], Alexey Smirnov[a], Joana Smirnovienė[a], Janis Leitans[c], Andris Kazaks[c], Kaspars Tars[c], Lena Manakova[d], Saulius Gražulis[d], and Daumantas Matulis[a]**

[a] Department of Biothermodynamics and Drug Design, Institute of Biotechnology, Life Sciences Center, Vilnius University, Saulėtekio 7, Vilnius LT-10257, Lithuania

[b] Department of Bioinformatics, Institute of Biotechnology, Life Sciences Center, Vilnius University, Saulėtekio 7, Vilnius LT-10257, Lithuania

[c] Latvian Biomedical Research and Study Centre, Ratsupites 1 k-1, Riga LV-1067, Latvia.
[d] Department of Protein-DNA Interactions, Institute of Biotechnology, Life Sciences Center, Vilnius University, Saulėtekio 7, Vilnius LT-10257, Lithuania

Corresponding Author

*E-mail: daumantas.matulis@bti.vu.lt, matulis@ibt.lt. Phone +370-5-223-4364. Fax. +370-5-223-4367

KEYWORDS: Drug design; intrinsic binding affinity; benzenesulfonamide; carbonic anhydrase; docking; structure-affinity relationship

ABBREVIATIONS: AZM, acetazolamide; BSA, benzenesulfonamide; CA, carbonic anhydrase; DNS, dansylamide; FTSA, fluorescent thermal shift assay; ΔG_{intr}, intrinsic standard Gibbs energy change upon binding; K_d, observed equilibrium dissociation constant; $K_{d,intr}$, intrinsic equilibrium dissociation constant; 2-NSA, naphthalene-2-sulfonamide; SFA, stopped-flow assay.

ABSTRACT

In the design of high-affinity and enzyme isoform-selective inhibitors, we applied an approach of augmenting the substituents attached to the benzenesulfonamide scaffold in three ways, namely, substitutions at the 3,5- or 2,4,6-positions, or expansion of the condensed ring system. The increased size of the substituents determined the spatial limitations of the active sites of the twelve catalytically active human carbonic anhydrase (CA) isoforms until no binding was observed due to inability of the compounds to fit in the active site. This approach led to the discovery of high-affinity and high-selectivity compounds for the anticancer target CA IX and antiobesity target CA VB. The X-ray crystallographic structures of compounds bound to CA IX showed the positions of the bound compounds, while computational modeling confirmed that steric clashes prevent the binding of these compounds to other isoforms and thus avoid undesired side effects. Such an approach, based on the Lock-and-Key principle, could be used for the development of enzyme-specific drug candidate compounds.

STATEMENT OF SIGNIFICANCE

In the design of isoform-selective enzyme inhibitors, a series of homologous compounds with augmented substituent groups was designed. Larger inhibitors bound with greater affinity until reaching a limit of accommodation to the active site followed by an abrupt decrease in affinity upon further augmentation of the substituent thus demonstrating the validity of the lock-and-key principle in determining the affinity and selectivity of protein – ligand recognition.

INTRODUCTION

Compounds may bind to proteins via different mechanisms ranging from a rigid ‘lock-and-key’ to flexible ‘induced fit’ or ‘conformational selection’(1, 2) modes. The induced fit emphasizes ligand ability to alter protein structure and dynamics upon binding. The ligand-bound and ligand-free states of a protein would differ significantly. The conformational selection, however, postulates that protein exists in multiple conformational states in solution and the ligand selects and binds to the most favored conformation. In this case ligand binding does not ‘induce’ a conformational change. On the other hand, the lock-and-key principle may be valid when the protein is conformationally rather rigid and does not substantially change its structure upon ligand binding. In this case, it is important to design ligands that would fit the active site pocket of the disease target protein being not too small and not too large in size to fit the pocket as closely as possible.

Herein, we designed a series of compounds of increasing sizes until the ligand compound could not fit in the active site and the affinity dropped thousands-of-fold. Modulating the size of the ligand yielded both high-affinity and high-selectivity compounds, and the principle could be applied to drug design to a much greater extent than currently used. To demonstrate this approach, we have used a family of enzymes that possesses the following important features: a) a

family consists of twelve structurally highly similar isoforms (isozymes) with essentially the same fold, b) the active site pocket of all isoforms is highly similar, differing from each other by only several amino acids, and c) the Zn(II) metal ion, bound in tetrahedral geometry to four nitrogen atoms, three protein histidines and the nitrogen of sulfonamide group, forming a coordination bond between the ligand and protein, increasing the affinity, orienting the ligand and allowing the prediction of how to increase the molecule size to fully fit the active site pocket.

The family of zinc metalloenzymes used in this study is carbonic anhydrase (CA), an enzyme that catalyzes the reversible hydration of CO_2 and maintains various physiological functions in essentially every cell of any living organism from bacteria to humans. Humans express fifteen CA isoforms, but only twelve of these forms contain Zn(II) and are catalytically active (3, 4). The 12 active isoforms have different subcellular localizations and can be found as cytosolic (I, II, III, VII and XIII), mitochondrial (VA and VB), extra-cellularly oriented but membrane-bound via a trans-membrane helix (IX, XII and XIV) or via a lipid anchor (IV) and secreted (VI). Some of these isoforms have been therapeutic drug targets for decades and are currently used as targets for the development of anti-glaucoma, diuretic, anti-obesity, and anti-convulsant drugs. The isoforms CA IX and CA XII have emerged as possible targets against cancer (5–8). However, many of the current clinical CA inhibitors, mostly used to treat glaucoma and high altitude sickness, demonstrate little selectivity for a particular CA isoform and, as a consequence, indiscriminately inhibit most of the isoforms.

The first CA was purified in 1933(9), while the first determination that sulfonamides inhibit CA was made in 1940 (10). The first X-ray crystal structure of a carbonic anhydrase was solved by Liljas et al in 1972 showing the presence of Zn(II) in the active site(11–13). The removal of Zn(II) from the native holoCA II decreased the affinity of primary sulfonamides to apoCA II (missing Zn(II)) by approximately 6 kcal/mol (14). The Whitesides group determined that approximately -8 kcal/mol of benzenesulfonamide binding energy is contributed by the Zn-N bond and only -1 kcal/mol by the hydrogen bonding network. The contacts between CA II and the un-substituted benzene ring contributed only -2.9 kcal/mol (15). The introduction of substituents on the benzene ring could significantly influence the orientation and binding mode of compounds in the active site and consequently strengthened the interaction with CA and enabled the generation of inhibitors with increased affinity and selectivity for several CA isoforms (16).

The group of R. McKenna has made significant efforts into designing human CA isoform-specific inhibitors by determining and reviewing the X-ray crystallographic structures of CA-ligand complexes (4, 17, 18). The deepest part of the active site pocket has been called the “conserved pocket” due to high similarity among isoforms. A group of amino acids that differ among isoforms and could form a basis for selective recognition has been called a “selective pocket” and is situated somewhat further from the active site. Any ligand has to make contacts with those amino acids to exhibit a selective binding profile. Furthermore, differences in amino acids change the pocket size as well as the maximal ligand sizes that can be accommodated.

Isoforms CA I and CA II exhibit more occluded active site entrance than CA IX and CA XII (CA I and CA II have Tyr204 and Phe131 at the entrance of the binding pocket, while CA IX and CA XII have Val131 and Ala131 at isostructural positions) and these differences have been used to design selective inhibitors [5,20].

In addition, selective inhibitors have been made by exploiting different subcellular locations of CAs. This strategy was especially useful to increase compound selectivity for extracellularly bound CA IX and CA XII by making membrane-impermeable inhibitors by the addition of cationic or other groups (7, 19, 20).

We have previously designed a series of fluorinated benzenesulfonamides bearing substituents at the *para*, *para*/*ortho* and *para/meta* positions with respect to the sulfonamide group (21–23) and concluded that bulky hydrophobic groups at the *ortho* or *meta* positions are crucial for selectivity towards CA IX. For example, compound VR16-09 bearing a bulky aminocyclododecyl group at the *ortho* position and another polar tail at the *para* position exhibited a selectivity that was more than a million-fold higher for CA IX than for CA I and CA II (23). Crystallographic studies rationalized the selectivity of the compound, showing that the bulky 12-member carbon ring occupies the hydrophobic part of the CA IX active site, whereas binding to CA II was not favorable due to the clash with Phe131 (24).

CA isoforms are relatively rigid enzymes and based on crystallographic data seem to not undergo substantial conformational changes upon ligand binding. Recently we have compared 24 crystal structures of CA isoforms in the absence and presence of various benzenesulfonamides.(25) The resultant RMSD values of peptide backbone between proteins without inhibitor and complexes with inhibitor were in the range of 0.17–0.51 Å showing that no significant conformational changes occured upon ligand binding. Other studies reviewed in (16) showed the RMSD around 0.2–0.4 Å between ligand-free and ligand-bound forms of CA II.

Here, we have synthesized di-*ortho*- and di-*meta*-substituted benzenesulfonamides with hydrophobic substituents of a systematically increasing size. The augmentation of the inhibitor size allowed determination of the maximal contact area and maximal size that could fit in the protein pocket. Variation of the substituent size and bulkiness allowed us to explore the features of CA active site cavities, giving new insights into the rational design of CA selective inhibitors.

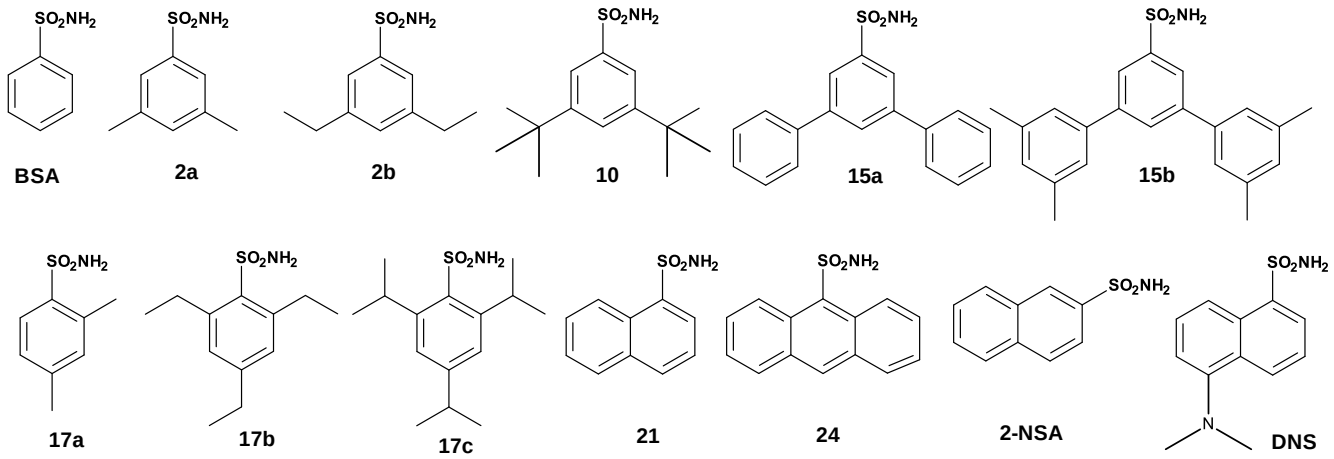

Figure 1. Series of benzenesulfonamide-bearing compounds designed for probing of CA enzyme active sites. Top line includes di-*meta*-substituted benzenesulfonamides while the bottom line shows the tri-substituted (di-*ortho* and *para*) benzenesulfonamides and ligands containing conjugated benzene ring systems. Compound synthesis is described in the Supporting Material.

MATERIALS AND METHODS

Protein preparation

Production and purification of twelve catalytically active human CA isoforms (CA I, II, III, IV, VA, VB, VI,VII, IX, XII, XIII and XIV) was performed as previously described(26). The catalytic domain of CA IX used for co-crystalization with inhibitor was produced in methylotrophic yeast *Pichia pastoris* as described in (27).

The purity of all recombinant CAs was analyzed by SDS-PAGE, and the molecular weights were confirmed by HR-MS.

Fluorescent thermal shift assay

Thermal shift assay (FTSA) determinations of compound affinities were performed by heating the protein samples containing various concentrations of an inhibitor from 25 to 99 °C while recording extrinsic fluorescence of the solvatochromic dye ANS (8-anilino-1-naphthalene sulfonate) and determining the protein melting temperatures at each compound concentration by fitting the melting curves to a two-state model of the protein unfolding (28, 29). The resultant melting temperatures were plotted as a function of added ligand concentration, and the binding constants were obtained according to the model taking into account the thermodynamics of protein unfolding and ligand binding (28, 29).

The FTSA experiments were performed in a Corbett Rotor-Gene 6000 (QIAGEN Rotor-Gene Q) instrument using the blue channel (excitation 365±20 nm, detection 460±15 nm). Samples contained 5-10 μM protein, 0-400 μM ligand, 50 μM ANS and 50 mM sodium phosphate buffer containing 100 mM NaCl at pH 7.0, with a final DMSO concentration of 2%. The applied heating rate was 1 ºC/min. All experiments were repeated at least twice.

Stopped-flow CO_2 hydration assay

Carbonic anhydrase inhibition experiments were performed by applying the stopped-flow CO_2 hydration assay (SFA) by using an Applied Photophysics SX.18MV-R stopped-flow spectrophotometer at 24 °C. Reaction buffer contained 25 mM Hepes, 0.2 M sodium sulfate and 50 μM Phenol Red indicator (λ - 557 nm), pH 7.5. Saturated CO_2 solution was prepared by bubbling the CO_2 gas in Milli-Q water for 1 h at 24 °C. Enzyme concentration was 200 nM for CA I, 50-100 nM for CA II, 300 nM for CA III, 100-200 nM for CA IV, 113 nM for CA VA, 264-300 nM for CA VB, 100 nM for CA VI, 50 nM for CA VII, 10-50 nM for mammalian CA IX, 150 nM for yeast CA IX, 50-200 nM for CA XII, 200-500 nM for CA XIII, and 40-45 nM for CA XIV. Inhibitor concentration was 0-150 μM (in a row of two-fold or three-fold serial dilution) in ≤1.5 % DMSO. Raw curves were fitted using a single exponential model and the inhibition constants were determined using the Morrison equation:

$$CA\ act.(\%) = 1 - \frac{([CA] + [I] + IC_{50} - \sqrt{([CA] + [I] + IC_{50})^2 - 4[CA][I]})}{2[CA]} \cdot 100\%$$

where [CA] is the total added CA concentration assuming that it is equal to the active enzyme concentration, [I] is the total added inhibitor concentration, and IC_{50} is the concentration of inhibitor that achieves 50% inhibition of the enzymatic activity. Fixed CA concentration was used to fit dose-response curves.

Determination of the pK_a of compound sulfonamide group

Compound was added to a series of 100 mM buffer solutions (ranging from pH 7.5 to 12.0 at every half pH unit) at the concentration of 60-200 μM, containing 2% DMSO. The UV-VIS spectra were recorded of each compound buffer solution at 25 ºC. The ratio of normalized absorbances (typically 10 nm above and below the isosbestic point) was plotted as a function of pH. The pK_a value was determined by fitting the curve to the Hendersson-Hasselbach equation. The pK_a values determined at 25 ºC were recalculated to 37 ºC by using the van't Hoff equation.

Intrinsic binding thermodynamics

Experimentally observed affinity constants and the IC_{50} values or inhibition constants K_i are dependent on variables such as pH because of ligand binding-linked protonation/deprotonation reactions occurring simultaneously with inhibitor binding. These dependencies may mislead the

chemical reasons for the structure-affinity relationships. Therefore, the experimentally observed constants are called "*observed*", and these constants should not be used to explain the compound structural reasons for drug design as previously explained (30). Instead, the intrinsic binding constant $K_{b,intr}$ should be calculated by dividing the experimentally determined observed binding constant K_b by the available fractions of deprotonated inhibitor and protonated Zn(II)-bound water form of CA:

$$K_{b,intr} = \frac{K_b}{(f_{RSO_2NH^-} f_{CAZnH_2O})} \quad (1)$$

The fractions of the deprotonated inhibitor and the Zn(II) bound water form of CA depend on the pK_a of the sulfonamide amino group (pK_{a_sulf}) and the pK_a of the water molecule attached to Zn(II) in the active site of CA (pK_{a_CA}), respectively:

$$f_{RSO_2NH^-} = \frac{10^{pH-pK_{a\_sulf}}}{1+10^{pH-pK_{a\_sulf}}} \quad (2)$$

$$f_{CAZnH_2O} = 1 - \frac{10^{pH-pK_{a\_CAZnH_2O}}}{1+10^{pH-pK_{a\_CAZnH_2O}}} \quad (3)$$

The pK_a values of water molecules coordinated to Zn(II) in the active site of CA isoforms were taken from the following (30): CA isoform – pK_a: CA I – 8.1, CA II – 6.9, CA III – 6.5, CA IV – 6.6, CA VA – 7.3, CA VB – 7.0, CA VI – 6.0, CA VII – 6.8, CA IX – 6.6, CA XII – 6.8, CA XIII – 8.0, and CA XIV – 6.8).

The intrinsic Gibbs energy of binding was calculated using eq (4):

$$\Delta G_{intr} = -RT \ln(K_{b,intr}) \quad (4)$$

The maps listing the intrinsic Gibbs energies of compound binding to each isoform and the differences after applying functional group additions are shown in Supporting Material Figures S4 and S5. The intrinsic $K_{d,intr}$ values for all CA isoforms are presented in Table S1. It is important that intrinsic rather than observed values are listed. However, the observed affinities are listed in Table 1 for the convenience of the reader who is accustomed to evaluating the observed constants at particular experimental conditions, such as pH 7.0.

Molecular docking *in silico*

Molecular docking was performed using Smina (31), an AutoDock Vina (32) because it supports a variety of scoring functions, including user-defined custom ones. Vinardo scoring function (33) was employed during the docking. Because of the importance of coordination bond between Zn(II) and sulfonamide nitrogen, a pseudo-atom was generated using AutoDock4$_{Zn}$ tool (34) at a tetrahedral Zn(II) coordination site, and an additional quadratic potential between the generated pseudo-atom and the sulfonamide nitrogen with –10 weight was added on top of the default Vinardo scoring function. 22.5×22.5×22.5 Å^3 size grid box was used during the docking. The search exhaustiveness during the docking was increased to 50 instead of the default 8. After the docking, the lowest energy docked pose was rescored using the unmodified Vinardo scoring function (33), as well as Convex-PL v. 0.3 scoring function (35). The human carbonic anhydrase isoforms CA VA and CA VB which did not have structures in Protein Data Bank (PDB) were

built using SWISS-MODEL web server (36), based on murine CA V template (PDB ID: 1KEQ). For the rest of catalytic human CAs, the receptor models were taken from the PDB (chain A except where noted): 1AZM (CA I), 3HS4 (CA II), 3UYQ (CA III), chain C of 5JN8 (CA IV), 3FE4 (CA VI), 6H38 (CAVII), 3IAI (CA IX), 1JD0 (CA XII), 3CZV (CA XIII), and 4LU3 (CA XIV). In the PDB structure 3FE4 of CA VI the magnesium ion was present instead of zinc, therefore it was replaced by Zn for the purposes of docking. Additional dockings were also performed into CA VI-mimic, PDB ID: 6QL2 (37). The receptor was kept rigid during the docking, except for the cases noted in the text in which one or two specified side chains were mobilized. The protein structures were prepared using UCSF Chimera, v. 1.13.1(38). The ligands were optimized using MMFF94s force field (39) within Avogadro program, v. 1.2.0 (40). The conversions of the files into various formats was done with AutoDock Tools, 01.26.2015 version (labeled as "latest") (41) and Open Babel v. 2.4.1 (42). Open Babel Application Programming Interface (API) was used to calculate heavy atom RMSDs between the docked and X-ray structures.

Crystallization of CA – compound complexes

The proteins were concentrated by ultrafiltration to 20-38 mg/mL (CA II), 25 mg/mL (CA XII) and 10 mg/mL (CA IX prepared in yeast). Crystallization conditions (buffers) are listed in Supporting Material- Table S6. The ligand solutions for crystal soaking were made by mixing of 50 µL of corresponding reservoir solution and 0.5 µL of 50 mM ligand solution (in DMSO). In the case of CA IX, the ligands were added via co-crystallization. The protein was incubated for an hour in a 5 mM ligand solution dissolved in DMSO before mixing it with the crystallization buffer.

X-ray data collection and structure determination

Two datasets of CA II-17a, CA II-2-NSA were collected at the EMBL (DESY, Hamburg, Germany) beamline P14, four datasets CA II-2a, CA II-24, CA XII-10, CA XII-15a – at beamline P13, CA II-21 at beamline X11. The dataset of CA IX-15a was collected at BESSY II (Berlin, Germany) beamline 14.1 and CA IX-2NSA at MAX IV (Lund, Sweden) beamline BioMAX. Most of the datasets were processed using XDS (43) program, whereas datasets of CA II-21, CA IX-15a – by MOSFLM (44). The molecular replacement was made by MOLREP (45) program using the following initial models: 3HLJ for CA II, 1JD0 for CA XII and 6FE2 for CA IX. The 3D models of compounds were created using AVOGADRO (40) program. The library files which contain complete chemical and geometric descriptions of compounds were created using LIBCHECK program (46). The models were prepared using COOT (47) and refined by REFMAC (48). All represented graphics were made using PyMOL programs (PyMOL, version 1.8.x). Coordinates and structure factors have been deposited to the RCSB. Data processing, refinement, and validation statistics are shown in Supporting Material- Table S3.

RESULTS

Compound binding and structure-affinity relationship

The binding of synthesized compounds to twelve catalytically active human CA isoforms was determined by the fluorescent thermal shift assay (FTSA). The K_d values for all compounds are listed in Table 1. Since FTSA only demonstrates binding and does not determine inhibition of enzymatic activity, the compound inhibitory properties were confirmed by the stopped-flow enzymatic inhibition of the CO_2 hydration assay (SFA) (data are listed in the parentheses in Table 1).

Table 1. The *observed* dissociation constants K_d (μM) for compound interaction with human recombinant CA isoforms are listed as determined by FTSA at 37 °C and pH 7.0. For comparison, the dissociation constants K_d (μM) were determined from the IC_{50} values obtained by the stopped-flow CA inhibition assay (SFA) at 24 °C and pH 7.5 (SFA data are listed in the brackets).

Cmpd	Dissociation constants K_d (μM) of CA isoforms											
	CA I	CA II	CA III	CA IV	CA VA	CA VB	CA VI	CA VII	CA IX	CA XII	CA XIII	CA XIV
BSA	7.1	1.8	>400	17	8.3	33	14	6.7	1.5	13	7.5	8.7
2a	21	18	>400	28	17	2.5	110	25	8.3	83	6.3	5.0
2b	67	3.8	>400	6.7	>400	0.13	33	4.6	0.33 (1.9)	17	0.91	1.7
10	>200	2.5 (1.25)	>200	11	>200	4.4	83	2.0	0.056 (0.18)	5.9 (1.1)	0.50	1.4
15a	>200	58 (>100)	>400	1.3	>400	>400	125	>400	0.0065 (0.067)	0.83 (0.50)	1.4	0.40
15b	>200	>200 (>100)	>200	>200	>200	>200	>200	>200	0.091 (0.33)	>200	>200	>200
17a	29	14	>600	50	25	18	125	50	17	100	17	5.0
17b	>400	>400	>400	>400	>400	100	>400	>400	50	>400	>400	10
17c	>400	>400	>400	>400	>400	>400	>400	>400	>400	>400	>400	>400
21	2.6	2.9	>400	2.5	3.3	0.83	5.0	1.6	0.33	2.5	0.83	0.56
24	>400	6.7	>400	5.0 (5.9)	>400	0.067 (<0.15)	8.3	10	1.0 (1.1)	9.8 (12.5)	1.3	1.3 (1.1)
2-NSA	0.91	0.77	>400	10	13	5.0	17	2.2	0.24 (0.13)	6.3	5.0	0.29
DNS	0.40 (<0.05)	2.0 (2.5)	>400	1.9 (0.67)	10 (2.8)	1.0 (4.0)	12.5 (5.0)	3.2 (1.7)	0.0040 (<0.015)	0.50 (0.03)	0.50 (<0.1)	0.17 (0.22)
AZM(30)	2.4 (0.29)	0.046 (0.010)	40	0.087	0.84	0.14	0.22	0.013	0.021 (0.0067)	0.13 (0.025)	0.12 (<0.01)	0.063

Uncertainties of the FTSA and SFA measurements are approximately 1.6-fold in K_d

Augmentation of substituents was performed on the benzenesulfonamide scaffold in three directions: 1) substituting 3,5-positions, 2) substituting 2,4,6-positions, and 3) extending the condensed ring system, having a significant effect on the binding affinities to the CA isoforms (Figure 2). Substitution of 3,5-positions had an important effect on CA IX, an anticancer drug target, binding profile. The affinity towards CA IX increased some 10-fold when changing from methyl (**2a**) to ethyl (**2b**), to tert-butyl (**10**) and to phenyl (**15a**) modifications, from 8300 nM to 330 nM, to 56 nM and 6.5 nM, respectively (Figure 2A). The last modification of 3,5-diphenyl groups (**15a**) to 3,5-dimethylphenyl groups (**15b**) decreased the affinity for CA IX by a factor of 10 (K_d = 91 nM). However, the bulky **15b** did not bind to any other CA isoform, making it the most selective for CA IX in the whole series of compounds presented in this study. Its selectivity for CA IX exceeded 2000-fold compared to that for any other isoform.

The second series of compounds involved variation of the length and the branching of the alkyl chain in the 2,4,6- positions in benzenesulfonamide (**BSA)**. Compounds bearing methyl (**17a**), ethyl (**17b**), and isopropyl (**17c**) groups were investigated. Unexpectedly, methyl substitution with ethyl led to the almost completely inactive compound **17b**. Compound **17c** with isopropyl groups failed to bind any CA isoforms indicating that two isopropyl substituents in *ortho* positions make it impossible for the sulfonamide to find a binding-suitable position in any CA isoform. It also means that the active site arrangement is rather rigid. Since the binding affinity is substantially reduced with the size of the substituent at the 2,4,6- positions (methyl < ethyl < isopropyl), the available space for the ligand is increasingly limited.

In the third series of compounds containing fused aromatic rings, the bulkiest anthracene-9-sulfonamide **24** was found to be a nanomolar inhibitor of CA VB (K_d = 67 nM), selective over the remaining CAs where the affinity was micromolar or lower.

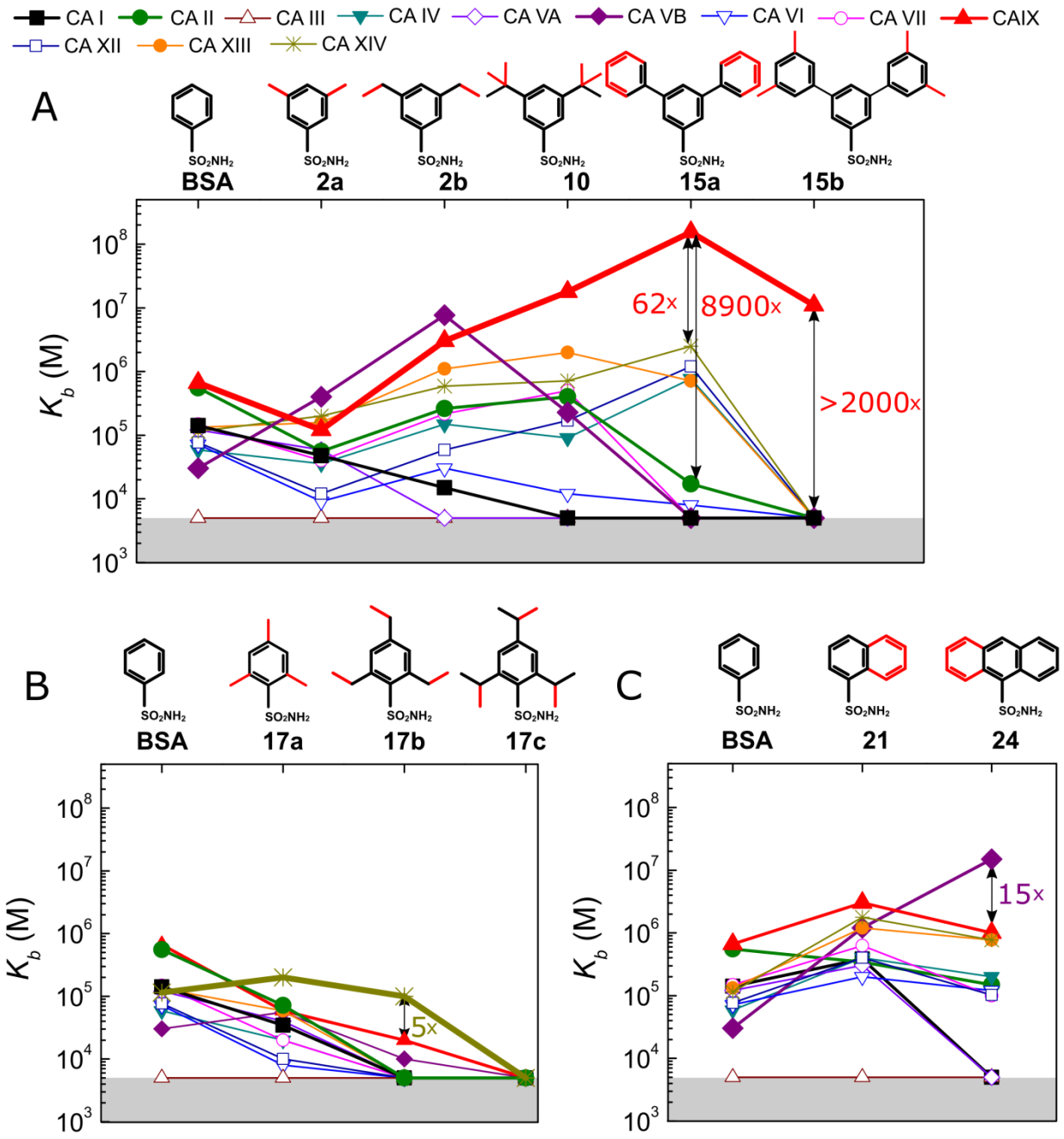

Figure 2. The observed binding constants of compound interactions with twelve CA isoforms of 3,5-substituted compounds (A), 2,4,6-substituted compounds (B) and ligands with fused benzene rings (C). Compound structures are shown on the top of each panel, and the gradual increase in the compound size and hydrophobicity compared with that of the neighboring compound is shown in red. A higher position means greater affinity, and the ratios of affinities (colored numbers inside the plots) show the selectivity over other isoforms. The gray area at the bottom of each plot shows the limit of detection of the assay.

Overall tendency was that the substituents of increased size bound with higher affinity, presumably due to better contacts with the protein until they filled the available space. Further increase in the size of the compound led to a sharp decrease in affinity due to inability to fit in the active site.

To investigate the structure-affinity relationship, intrinsic dissociation constants ($K_{d,intr}$) and intrinsic Gibbs energy (ΔG_{intr}) values for interactions between CA isoforms and compounds were calculated (Tables S1, S2, Supporting Material). The intrinsic parameters represent the actual binding reaction between the sulfonamide with a deprotonated amino group and the Zn-bound water form of CA. Such a binding reaction has been confirmed by neutron diffraction crystallography as the reaction taking place when sulfonamides bind to CA(49–51). In the compound structure-affinity correlation analysis, only intrinsic parameters are meaningful, providing insight into molecular recognition.

Using ΔG_{intr} values, we constructed compound structure-affinity correlation maps (Figure 3 and Figure S3 (Supporting Material)). The modification of the simplest compound **BSA** by introducing hydrophobic substituents at di-*meta* positions in the direction of **2a→2b→10→15a** was the most favorable for CA IX, with the absolute value of ΔG_{intr} gradually increasing from -54.1 kJ/mol for **2a** to -71.9 kJ/mol for **15a**. Compound **15a** with the diphenyl groups at the *meta* positions of benzenesulfonamide was the strongest binder of CA IX ($K_{d,intr}$ of 0.8 pM). Compound **15a** was the optimal compound for efficient CA IX inhibition, and further modification to **15b** was unfavorable for binding to CA IX and all other CAs.

The binding affinity increased slightly for CAs in the direction **2a→17a** (dimethyl→trimethyl groups) but decreased for all isoforms in the direction **17a→17b→17c** (from trimethyl to triethyl and triisopropyl substituents), showing that such compounds are too bulky to fit in the active sites of CAs or that the positions of the two *ortho*-methyl groups make the arrangement of the inhibitor energetically unfavorable.

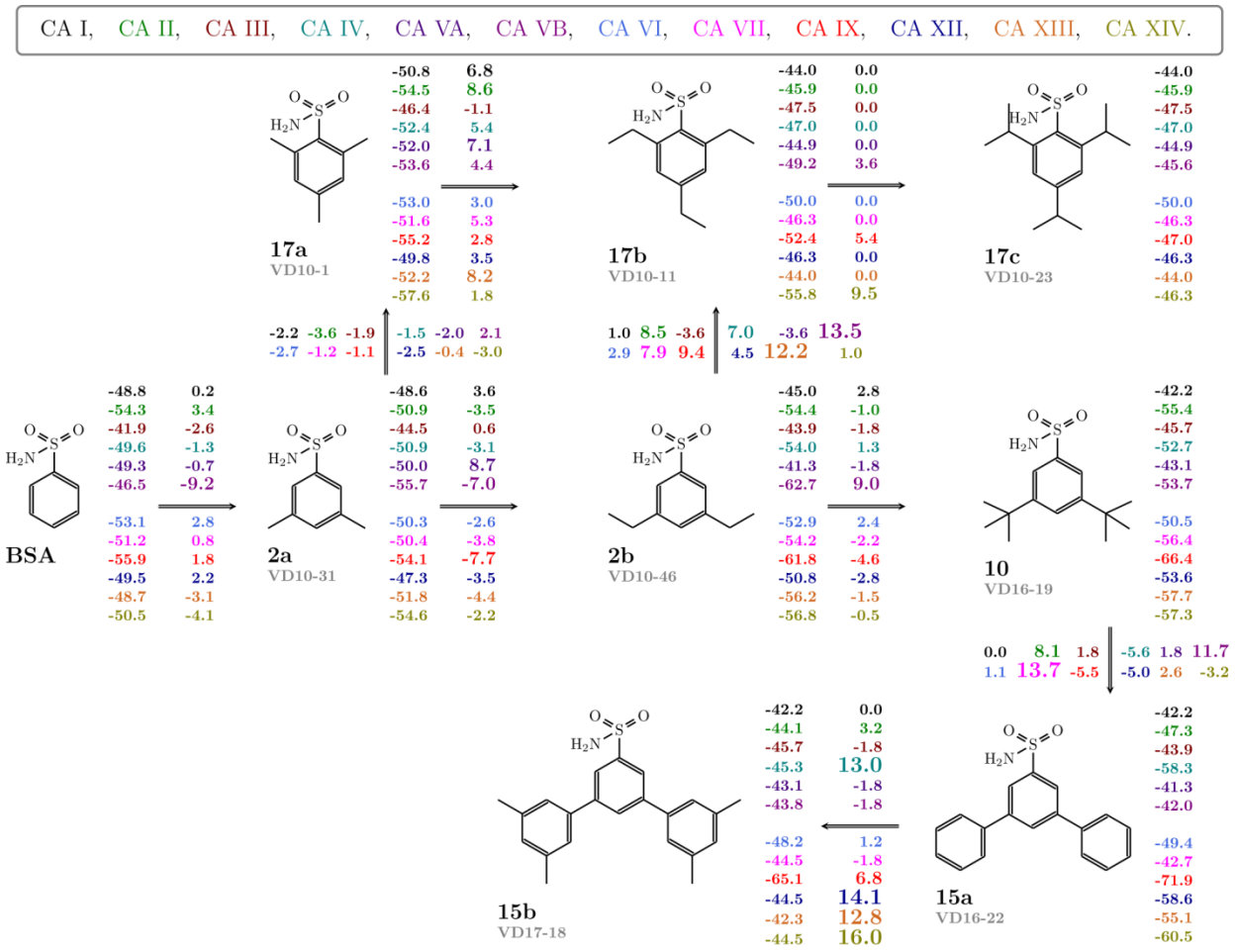

Figure 3. The map of correlations between the compound chemical structures and the intrinsic standard Gibbs energy changes upon compound binding to all 12 CA isoforms is shown. Chemical structures of compounds are listed according to their similarities while growing in molecular size in the direction of arrows. Intrinsic Gibbs energies of binding are listed next to the chemical structures. Differences in the intrinsic Gibbs energies upon binding between the structurally similar compounds are shown next to the arrows. The values are in kJ/mol. Negative values show tighter binding while positive values indicate weaker affinities. Colors represent the 12 catalytically active human CA isoforms. This map shows how small changes in compound structure lead to relatively large changes in the binding energy and at the same time provides the selectivity of binding to a particular CA isoform.

The interaction thermodynamics of the synthesized compounds with the twelve CA isoforms clearly showed that the active site cavities of the CA isoforms differ in volume and shape. The variation of substituent size and bulkiness in the benzene ring allowed us to determine the optimal inhibitor diameter and shape for the efficient inhibition of cancer-related isoform CA IX and mitochondrial CA VB, which is implicated in obesity-related pathologies.

X-ray crystal structures of compound-CA complexes

Nine X-ray crystallographic structures of the inhibitors bound in the active sites of several CA isoforms were determined to study the structure-thermodynamics correlations and the binding recognition (Figure 4 (and Figure S5 in the Supporting Material)). The structures show the most energetically favorable orientations of the bound ligand. In each case, the sulfonamide amino group formed a direct coordination bond with the Zn(II) while the hydrophobic part of each compound was exposed to the solvent.

CA II exhibits a narrower active site than CA IX because CA II contains Phe131 instead of Val (Figure 4). The limitation of the size of the binding pocket was likely the main reason for the differences in the binding affinities of bulky compounds to CA II and CA IX.

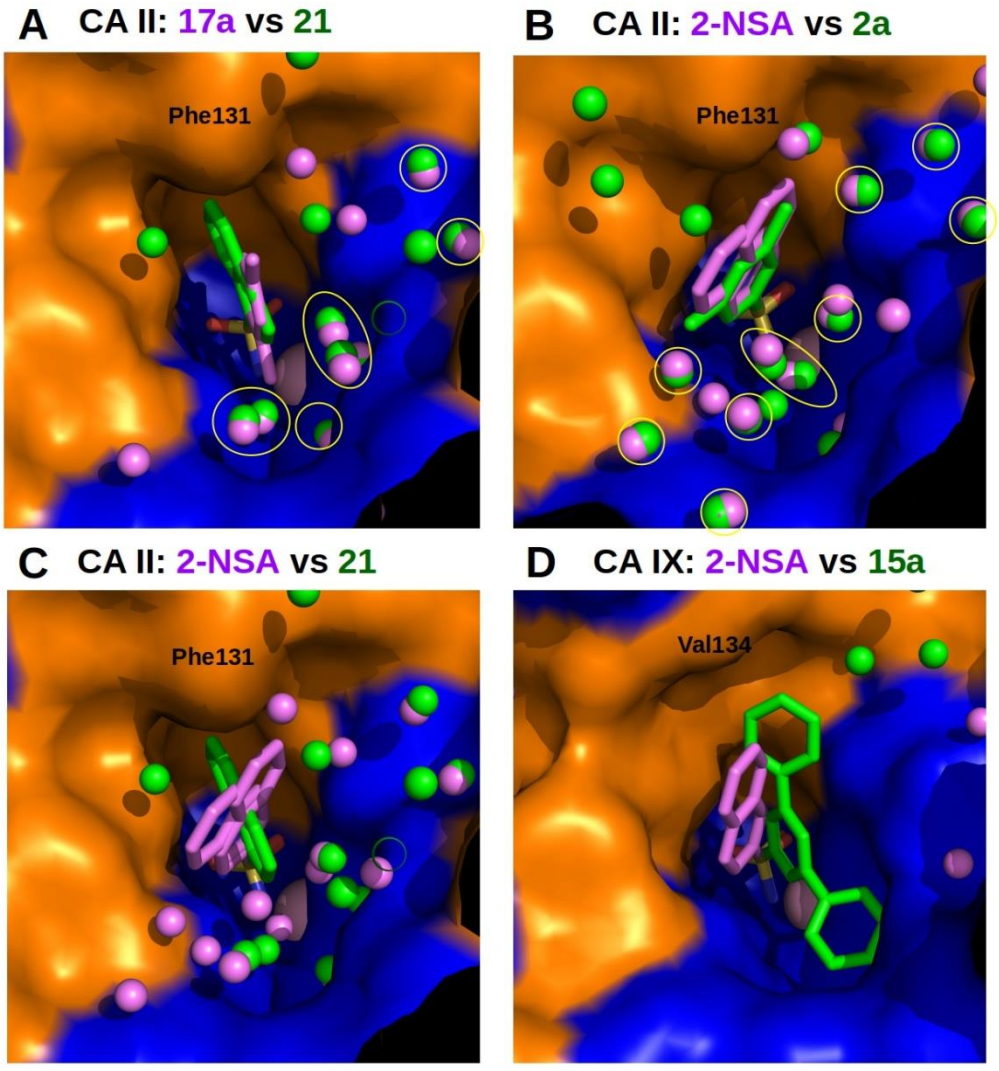

Figure 4. Pair-wise comparison of the structural arrangement of related compounds bound to CA II and CA IX as determined by X-ray crystallography. Inhibitors bound to CA II are all shown in

the same orientation. The structures and names of the inhibitors in pairs are shown in pink or green. Water molecules found in corresponding crystal structures are shown as green or pink spheres. The Zn(II) ion is shown as a pink sphere at the bottom of the active site. The CA protein surface is colored orange for hydrophobic residues (Val, Ile, Leu, Phe, Met, Ala, Gly, and Pro) and blue for residues with charged and polar side chains (Arg, Asp, Asn, Glu, Gln, His, Lys, Ser, Thr, Tyr, Trp, and Cys). (A) Compounds **17a** (PDB ID 6T4N, pink) and 21 (PDB ID 6T4P, green) bound to the active site of CA II. (B) Compounds **2-NSA** (two alternately oriented positions, PDB ID 6T81, pink) and **2a** (PDB ID 6T4O, green) bound to the active site of CA II. (C) Compounds **2-NSA** (two alternately oriented positions, PDB ID 6T81, pink) and **21** (PDB ID 6T4P, green) bound to the active site of CA II. (D) Compound **2-NSA** (PDB ID 6TL6, pink) and **15a** (PDB ID 6TL5, green) bound to the active site of CA IX. Electron-density maps, the refinement statistics and additional figures are provided in the Supporting Material.

The sulfonamide group of compounds **21** and **17a** bearing either the naphthalene ring (in **21**) or 2,4,6-trimethylbenzene (in **17a**) occupied similar positions in both crystal structures of CA II (Figure 4A). Both crystal structures had comparable resolutions of 1.4 Å and 1.8 Å, respectively, and therefore, the solvent molecules in both structures could be compared. Water molecules in the hydrophilic part of the active site in these structures could be found in very similar positions (marked by yellow circles in Figure 4). Sulfonamides **17a** and **21** had similar intrinsic binding affinities to CA II, the $K_{d,\mathrm{intr}}$ values were equal to 0.65 and 1.7 nM, respectively (Table S1). Interestingly, binding of compound **21** to CA II induced rotation of the Leu141 and Leu198 side chains to better accommodate the ligand in the binding site, compared to the Leu141 and Leu198 geometries in CA II complexes with compounds **17a, 2a**, **2-NSA** and **24**, solved in this study, as well as other smaller ligands, including **AZM** (PDB ID 3HS4) and **BSA** (PDB ID 6GDC).

The next pair of compounds to be compared is **2-NSA** and **2a** (Figure 4B). Naphthalene derivative **2-NSA** differed from **21** by the position of sulfonamide on the naphthalene ring, and benzenesulfonamide derivative **2a** differs from **17a** by the positioning of the methyl groups. The **2-NSA** in CA II was modeled by two alternate conformations, but the electron density of the second conformation (Figure S4A) is weak. Benzene rings of benzenesulfonamide of both compounds formed aliphatic-aromatic interactions with the side chain of residue Leu141. The positions of sulfonamides are similar in both crystal structures. The distribution of water molecules in the hydrophilic parts of the CA II active site was similar (Figure 4B), as were the conformations of the active site residues. The intrinsic binding affinities of both compounds were also comparable (Table S1, $K_{d,intr}$ 0.57 nM (**2-NSA**) vs 2.6 nM (**2a**)). Two alternate conformations of naphthalene derivative **2-NSA** could be due to a quasi-symmetry of the shape of the naphthalene ring when it is flipped around the sulfonamide C–S bond.

Figure 4C compares the binding modes of naphthalene derivatives **2-NSA** and **21** in CA II. These inhibitors differed by the position of sulfonamide on the naphthalene ring. Due to the fixed position of sulfonamide specifically bound to the zinc atom, the positions of the naphthalene substituent were determined by the geometry of the active site cavity. The narrower compound **2-NSA** was found in an alternate conformation in the crystal structure. The naphthalene ring of

compound **21** was located in the hydrophobic environment beneath the Phe131 side chain, whereas the naphthalene ring of compound **2-NSA** could not have the same orientation, as both alternate conformations should clash sterically with Phe131. Despite dissimilar orientations of naphthalene rings and different positions of water molecules, these compounds had comparable affinity to CA II ($K_{d,intr}$: 1.7 nM for **21** vs 0.57 nM for **2-NSA**, Table S1). The resolution of the crystal structure of CA II with the naphthalene derivative **2-NSA** was much better than of the complex with **21** (1.0 Å vs 1.8 Å, respectively). As shown in Figure 4C, compound **21** rather tightly filled the hydrophobic part of the active site cavity.

Figure 4D compares the binding mode between compounds **2-NSA** and **15a** in the active site of CA IX. The sulfonamide groups in both compounds were slightly tilted (the S-C bond was tilted by ~30°) with respect to each other due to spatial restraints imposed by the cavities on the hydrophobic ring systems. Compound **2-NSA** occupied the hydrophobic part of the active site of CA IX in a manner similar to that in complexes with CA II (Figure 4B or C). Sulfonamide **15a** more efficiently occupied the active site of CA IX, and the benzene ring of one *meta*-substituent was located in the hydrophilic part of the active site, where it displaced water molecules. The *meta*-terphenyl derivative **15a** bound to CA IX 143-fold stronger than the naphthalene derivative **2-NSA**. The $K_{d,intr}$ were 0.00077 and 0.11 nM, respectively (Table S1). The large difference between the two binding affinities was due to different binding modes and better filling of the binding pocket by compound **15a**. The displaced water molecules from the hydrophilic part of the active site could not reach the sulfonamide group during Zn(II)-**15a** dissociation as discussed in (52).

The binding mode of compound **15a** was similar in the active sites of CA XII and CA IX (compare Figure 4D (green) and Figure S5D (pink)). Compound **15a** bound significantly better to CA IX than to CA XII ($K_{d,intr}$ 0.00077 and 0.13 nM, respectively, Table S1). The active site of CA XII is more hydrophilic than that of CA IX (compare blue (hydrophilic) and orange (hydrophobic) surfaces in Figures 4D and S5D). The binding is weaker to CA XII than to CA IX likely due to hydrophobic compound **15a** binding to a more hydrophilic binding site of CA XII.

In silico docking of the compounds to the active sites of enzymes

Molecular docking can often give useful insight about the ligand-receptor structural arrangement, especially if the experimental structures are not available, and also provide the binding energy estimates. For this purpose, all studied compounds were docked to all 12 CA isoforms by using Smina(31), a fork of Autodock(32) , using Vinardo(33) and Convex-PL(35) scoring functions. In many cases, the best binders for the isoforms were correctly predicted by docking. The full analysis of the docking results can be found in Supporting Material. Below we describe some of the insights into the binding of two highest-affinity compounds for CA IX revealed by docking.

An example of the docked structures of CA IX-selective ligands **15a** and **15b** compared with the X-ray structure of **15a** in the CA IX binding site is shown in Figure 5. The picture displays

superposed solvent-accessible surfaces of CA IX with CA I (Figure 5A) and CA II (Figure 5B) and shows the clashes of CA I and CA II surfaces with the two terminal rings of the bifurcated ligand in panels C and D. Compounds **15a** and **15b** could not bind to CA I due to clashes with Phe91, Leu131, His67 and His200 or to CA II due to clashes with Phe131 and Asn67. The smaller Asn67 of CA II clashes with the ligand more than the bulkier Gln67 does in the same position in CA IX because Gln67 is flipped and its CO group forms a hydrogen bond with the amino group of Gln92. Interestingly, in some zones, CA IX is bulkier than CA I and CA II, but there are no clashes with the ligands. The docking in these cases fully reproduced the experimental crystallographic and thermodynamic binding data.

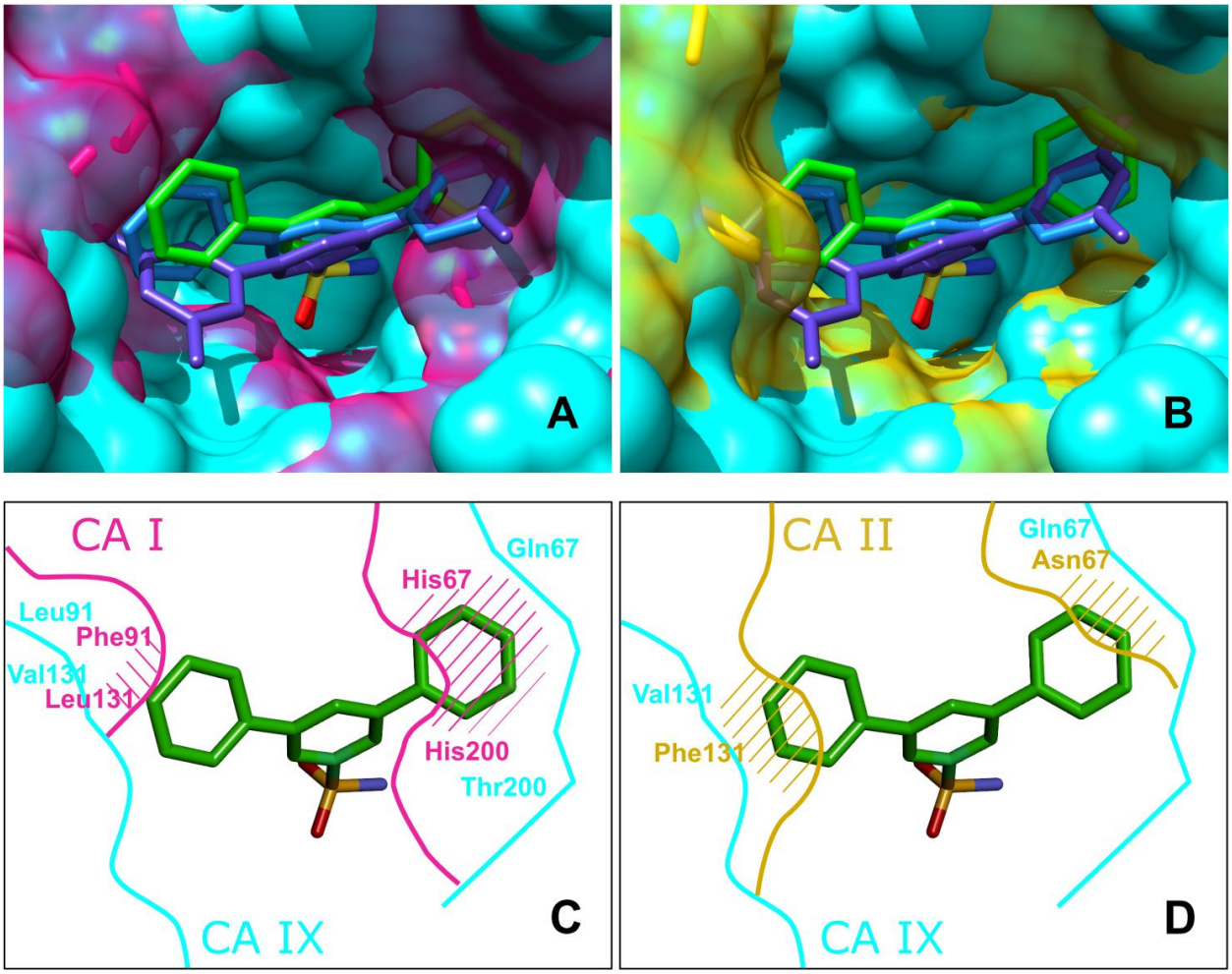

Figure 5. X-ray crystal structure of **15a** (green sticks) bound to CA IX (protein shown in opaque cyan surface) superimposed with the structures of CA I (pink) or CA II (yellow) showing that the compound cannot bind in the same orientation to either CA I or CA II due to steric clashes shown as dashed areas in the bottom panels. The docked orientations of two CA IX-selective compounds **15a** (blue sticks) and **15b** (purple sticks) to CA IX closely resembled the X-ray position of **15a**. The solvent-accessible surface for CA IX is shown as an opaque cyan surface.

The solvent-accessible surfaces of CA I (transparent pink in panel A) and CA II (transparent yellow in panel B) are shown, while the CA I and CA II protein atoms that extend out beyond the CA IX surface are visible as pink and yellow sticks. Panels C and D show compound **15a** in the same orientation as that in the crystal structure, while the protein surfaces of CA I and CA II (in the same coloring) show clashes with both terminal rings of the bifurcate ligands. The numbering of amino acids in CA I and CA IX is presented according to CA II. Correlations between experimentally determined and calculated binding affinities are provided in the Supporting Material (Figures S6-S7).

DISCUSSION

Despite the numerous studies concerning enzyme isoform-specific inhibitors, we do not have sufficiently well-defined tools for rational design of selective inhibitors. In this work, we present a method of CA isoform cavity investigation in which a benzenesulfonamide series with a substituted hydrophobic group of increasingly larger size was used. When the ligand size is incrementally increased, there ought to be a limiting size after which the molecule cannot fit into the binding site. This size limit should vary for every isoform and could be employed to search for isoform-selective inhibitors. Additionally, the aim was to increase the size of the ligand until hopefully it cannot fit in the binding pocket of some CA isoforms that we would not want to target. In particular, ubiquitous isoform CA II has a bulky Phe131 side chain pointing towards the binding site, while in clinically relevant isoform CA IX it is replaced by a smaller valine residue.

Variation of the substituent length and bulkiness was performed on the benzenesulfonamide scaffold by three approaches: 1) substituting 3,5-positions, 2) substituting 2,4,6-positions, and 3) extending the condensed ring system. This strategy proved to be successful and led to the discovery of several inhibitors specific for CA IX and CA VB. Promising CA IX inhibitors were revealed, namely, **15a** (observed K_d = 6.5 nM, 60-fold higher selectivity than that of the next best binding isoform), **10** (K_d = 56 nM, 9-fold higher selectivity), and **15b** (K_d = 91 nM, >2000-fold higher selectivity). For **15b**, no binding was detected to any other catalytically active CA isoform; it bound solely to CA IX. Anthracene-9-sulfonamide **24** turned out to be a selective inhibitor for CA VB (K_d = 67 nM, 15-fold selectivity).

Some other compounds among the investigated series appear to be promising scaffolds for further development. For example, compared to **BSA**, naphthalene-1-sulfonamide **21** and naphthalene-2-sulfonamide **2-NSA** bound better to most CA isoforms; therefore, compared to **BSA**, they could potentially be better lead compounds in designing new CA inhibitors, since the solved crystal structures with these compounds show that certain positions on these ligands could be advantageously expanded as substituents. **DNS** is an example of such improvement for **21**: the addition of a 5-(dimethylamino) group led to another selective nanomolar CA IX inhibitor (K_d = 4 nM, 40-fold higher selectivity).

It appears that the dominating mechanism or mode of action of the inhibitors followed the Lock-and-Key principle where the protein is structurally rather rigid and the conformations of the unliganded and ligand-bound protein are similar. The analysis of numerous available crystallographic structures of unliganded CA enzymes and enzyme-ligand complexes largely indicate that there is no major conformational change upon ligand binding (16, 25). However, a previous study has indicated otherwise and preferred to conclude that the binding mechanism is occurring primarily according to the conformational selection principle (53).

Searching for leads or improving their selectivity is a routine approach in drug discovery. However, to the best of our knowledge, systematic exploration by increasing the ligand size in search of the expansion limit for a particular CA isoform is a novel approach that has not been attempted before for enzyme inhibition. Certainly, this approach would not have been possible without the presence of a sulfonamide group, which serves as an 'anchor' group ensuring binding to the zinc ion situated in the deep cleft of the active site. The first and general rule was that the sulfonamide group had to achieve a favorable position for interaction in the active site of the CA isoform. The coordination bond between the nitrogen atom of the sulfonamide group and Zn(II) and the two hydrogen bonds between sulfonamide and the residues of the active site make the right conditions for tight interaction. Another part of the inhibitor is important for the formation of additional interactions between the inhibitor and active site of the protein and to some extent affects the binding geometry of the sulfonamide moiety. The successful results herein were obtained by using exclusively hydrophobic substituents (except the dimethylamino substituent in **DNS**) in benzenesulfonamides, which simplified the task by avoiding the concern about matching hydrogen bond donors and acceptors in the receptors, etc. On the other hand, the obtained selective inhibitors were merely frameworks consisting of carbon atoms, and the properties of the obtained leads can be further improved by substituting some of the carbon atoms with other elements (nitrogen, oxygen, etc.) or by attaching additional more finely tailored or hydrophilic substituents.

The use of large, bulky hydrophobic substituents is not new(54, 55). However, in similar cases, the hydrophobic groups targeted a specific position somewhere in the fringes of the binding pocket. In this study, the large hydrophobic group was targeted to fill the whole binding pocket as much as possible, to probe its limits and to discover essential differences between the isoforms.

The X-ray structure of the best binding compound/receptor combination **15a**-CA IX provided insights into the origin of the strong binding, as well as the selectivity towards CA IX. The bulky Phe131 side chain in CA II is replaced by a smaller valine side chain in CA IX, allowing for a good fit of compound **15a** in the CA IX binding site. CA XII has an even smaller alanine side chain in that position, and the **15a**/CA XII complex exhibited a binding mode similar to that of the complex with CA IX. However, the ~130-fold weaker binding of the hydrophobic ligand **15a** to CA XII than to CA IX was probably attributable to the more hydrophilic character of the binding pocket in CA XII than in CA IX.

X-ray crystallographic analysis of several compounds bound to CA II, CA IX and CA XII essentially confirmed that the most successful ligands nearly completely filled the binding site. X-ray crystallography confirmed that the selectivity of **15a** towards CA IX was due to the combination of the optimal size of the binding site at a strategically important distance from zinc, e.g., due to the decreased size of residue 131, which is mutated from Phe in many CA isoforms to Val in CA IX.

Since only some crystal structures involving investigated compound/receptor complexes were available, docking of all compounds to all CA isoforms was employed to test the extent to which we could predict the structural positions and the binding energetics. To obtain two slightly different results for the binding affinities, docking was performed using two scoring functions with different underpinnings (Vinardo is a physics-based fitting function, and Convex-PL is a knowledge-based potential). The docking calculations were able to correctly reproduce the binding modes of larger ligands, such as **24**, **10**, and **15a**, with mixed success in reproducing the binding modes of the smaller ligands. For the smaller ligands, it can be argued that the accurate reproduction of the binding mode was not essential for the success of the undertaken task of finding selective inhibitors since (a) the observed small ligand scores are relatively close to each other irrespective of geometry and (b) the small ligands turned out to have a low isoform selectivity and therefore were less interesting. For the important CA IX and CA XII isoforms, the docking essentially confirmed conclusions drawn from the X-ray structures. It is concluded that docking has a predictive capability that can be used to design better drugs.

CONCLUSIONS

Carbonic anhydrase model enzyme active site cavity was explored with sulfonamide ligands by gradually augmenting their hydrophobic substituents. The funnel-like binding pockets in the twelve catalytically active human CA isoforms were able to differently accommodate ligands containing hydrophobic substituents at the benzene ring of the sulfonamide. Benzenesulfonamides bearing bulky hydrophobic substituents at *meta* positions yielded promising CA IX inhibitors, and di-*meta* compounds filled well the CA IX active site cavity. Extension of the condensed ring system allowed the discovery of new CA VB-selective inhibitors. The application of di-*meta* compounds distinguished the CA IX isoform as having the most spacious active site cavity. In contrast, substitution of *ortho* positions with more bulky substituents than methyl groups led to loss of interaction, revealing a rather narrow “neck” of the CA active site cavities not far from the zinc ion. All these observations indicate that the primary mechanism of ligand binding occurs according to the rigid Lock-and-Key principle. Optimal inhibitor and active site cavity sizes appear to be of great importance for the design of novel selective inhibitors for CA enzymes, and the approach could find use in drug design for other ligand-enzyme systems.

SUPPORTING MATERIAL

Additional, detailed information for Results, Materials and Methods sections is given. Results subsections (Compound binding and structure-affinity relationship, X-ray crystal structures of compound-CA complexes, *In Silico* docking of the compounds to the active sites of enzymes) are described with additional tables and figures. Materials and Methods section consists of several subsections: Chemistry (description of compound synthesis); Compound characterization (description of experimental procedures); Crystallization of CA – compound complexes.

The Supporting Material is available free of charge via the Internet at http://doi.org.

AUTHOR CONTRIBUTIONS

V. D. and D. M. conceived and designed the experiments; V. D. performed the synthesis; A. Z. and J. S. performed the binding and inhibition studies; V.K. performed the molecular modeling studies; A. S., J. L., K. T., E. M. and S. G. performed and analyzed the X-ray crystallography data; A. K. produced CA IX in yeast; V. D., A. Z., V. K., A. S., and D. M. wrote the manuscript.

The manuscript was written through contributions of all authors. All authors have given approval to the final version of the manuscript.

ACKNOWLEDGMENT

This research was supported by the grant S-MIP-17-87 from the Research Council of Lithuania.

Authors thank Gleb Bourenkov and Guillaume Pompidor for the help with data collection at P14 and P13 EMBL beamlines at PETRA III ring of the DESY synchrotron. This work has been in part supported by iNEXT, grant number 653706, funded by the Horizon 2020 program of the European Commission.

REFERENCES

1. Holyoak, T. 2013. Molecular Recognition: Lock-and-Key, Induced Fit, and Conformational Selection. In: Roberts GCK, editor. Encyclopedia of Biophysics. Berlin, Heidelberg: Springer Berlin Heidelberg. pp. 1584–1590.

2. Boehr, D.D., R. Nussinov, and P.E. Wright. 2009. The role of dynamic conformational ensembles in biomolecular recognition. *Nat Chem Biol*. 5:789–796.

3. McKenna, R., and S.C. Frost. 2014. Overview of the carbonic anhydrase family. *Subcell Biochem*. 75:3–5.

4. Aggarwal, M., B. Kondeti, and R. McKenna. 2013. Insights towards sulfonamide drug specificity in α-carbonic anhydrases. *Bioorg Med Chem*. 21:1526–1533.

5. Chiche, J., J.-E. Ricci, and J. Pouysségur. 2013. Tumor hypoxia and metabolism -- towards novel anticancer approaches. *Ann Endocrinol (Paris)*. 74:111–114.

6. Monti, S.M., C.T. Supuran, and G. De Simone. 2012. Carbonic anhydrase IX as a target for designing novel anticancer drugs. *Curr Med Chem*. 19:821–830.

7. Singh, S., C. Lomelino, M. Mboge, S. Frost, and R. McKenna. 2018. Cancer Drug Development of Carbonic Anhydrase Inhibitors beyond the Active Site. *Molecules*. 23:1045.

8. Y. Mboge, M., R. McKenna, and S. C. Frost. 2016. Advances in Anti-Cancer Drug Development Targeting Carbonic Anhydrase IX and XII. In: Atta-ur-Rahman, K Zaman, editors. Topics in Anti-Cancer Research. Bentham Science Publishers. pp. 3–42.

9. Meldrum, N.U., and F.J.W. Roughton. 1933. Carbonic anhydrase. Its preparation and properties. *J. Physiol.* 80:113–142.

10. Mann, T., and D. Keilin. 1940. Sulphanilamide as a Specific Inhibitor of Carbonic Anhydrase. *Nature*. 146:164–165.

11. Liljas, A., K.K. Kannan, P.C. Bergsten, I. Waara, K. Fridborg, B. Strandberg, U. Carlbom, L. Jarup, S. Lovgren, and M. Petef. 1972. Crystal structure of human carbonic anhydrase C. *Nat. New. Biol.* 235:131–137.

12. Tilander, B., B. Strandberg, and K. Fridborg. 1965. Crystal structure studies on human erythrocyte carbonic anhydrase C. (II). *J. Mol. Biol.* 12:740–760.

13. Fridborg, K., K.K. Kannan, A. Liljas, J. Lundin, B. Strandberg, B. Strandberg, (The Late) B. Tilander, and G. Wirén. 1967. Crystal structure of human erythrocyte carbonic anhydrase C. *J. Mol. Biol.* 25:505–516.

14. King, R.W., and A.S. Burgen. 1976. Kinetic aspects of structure-activity relations: the binding of sulphonamides by carbonic anhydrase. *Proc R Soc Lond B Biol Sci*. 193:107–125.

15. Krishnamurthy, V.M., B.R. Bohall, C.-Y. Kim, D.T. Moustakas, D.W. Christianson, and G.M. Whitesides. 2007. Thermodynamic parameters for the association of fluorinated benzenesulfonamides with bovine carbonic anhydrase II. *Chem Asian J*. 2:94–105.

16. Krishnamurthy, V.M., G.K. Kaufman, A.R. Urbach, I. Gitlin, K.L. Gudiksen, D.B. Weibel, and G.M. Whitesides. 2008. Carbonic Anhydrase as a Model for Biophysical and Physical-Organic Studies of Proteins and Protein−Ligand Binding. *Chem. Rev.* 108:946–1051.

17. Pinard, M.A., B. Mahon, and R. McKenna. 2015. Probing the Surface of Human Carbonic Anhydrase for Clues towards the Design of Isoform Specific Inhibitors. *Biomed. Res. Int.* 2015:1–15.

18. Lomelino, C.L., J.T. Andring, and R. McKenna. 2018. Crystallography and Its Impact on Carbonic Anhydrase Research. *Int J Med Chem*. 2018:9419521.

19. Casey, J.R., P.E. Morgan, D. Vullo, A. Scozzafava, A. Mastrolorenzo, and C.T. Supuran. 2004. Carbonic anhydrase inhibitors. Design of selective, membrane-impermeant inhibitors targeting the human tumor-associated isozyme IX. *J. Med. Chem.* 47:2337–2347.

20. Supuran, C.T., A. Scozzafava, M.A. Ilies, B. Iorga, T. Cristea, F. Briganti, F. Chiraleu, and M.D. Banciu. 1998. Carbonic anhydrase inhibitors — Part 53. Synthesis of substituted-pyridinium derivatives of aromatic sulfonamides: The first non-polymeric membrane-impermeable inhibitors with selectivity for isozyme IV. *Eur. J. Med. Chem.* 33:577–594.

21. Dudutienė, V., A. Zubrienė, A. Smirnov, D.D. Timm, J. Smirnovienė, J. Kazokaitė, V. Michailovienė, A. Zakšauskas, E. Manakova, S. Gražulis, and D. Matulis. 2015. Functionalization of Fluorinated Benzenesulfonamides and Their Inhibitory Properties toward Carbonic Anhydrases. *ChemMedChem*. 10:662–687.

22. Dudutienė, V., J. Matulienė, A. Smirnov, D.D. Timm, A. Zubrienė, L. Baranauskienė, V. Morkūnaite, J. Smirnovienė, V. Michailovienė, V. Juozapaitienė, A. Mickevičiūtė, J. Kazokaitė, S. Bakšytė, A. Kasiliauskaitė, J. Jachno, J. Revuckienė, M. Kišonaitė, V. Pilipuitytė, E. Ivanauskaitė, G. Milinavičiūtė, V. Smirnovas, V. Petrikaitė, V. Kairys, V. Petrauskas, P. Norvaišas, D. Lingė, P. Gibieža, E. Capkauskaitė, A. Zakšauskas, E. Kazlauskas, E. Manakova, S. Gražulis, J.E. Ladbury, and D. Matulis. 2014. Discovery and characterization of novel selective inhibitors of carbonic anhydrase IX. *J. Med. Chem.* 57:9435–9446.

23. Kazokaitė, J., R. Niemans, V. Dudutienė, H.M. Becker, J. Leitāns, A. Zubrienė, L. Baranauskienė, G. Gondi, R. Zeidler, J. Matulienė, K. Tārs, A. Yaromina, P. Lambin, L.J. Dubois, and D. Matulis. 2018. Novel fluorinated carbonic anhydrase IX inhibitors reduce hypoxia-induced acidification and clonogenic survival of cancer cells. *Oncotarget*. 9.

24. Tars, K., and D. Matulis. 2019. X-Ray Crystallographic Structures of High-Affinity and High-Selectivity Inhibitor Complexes with CA IX That Plays a Special Role in Cancer. In: Matulis D, editor. Carbonic Anhydrase as Drug Target: Thermodynamics and Structure of Inhibitor Binding. Cham: Springer International Publishing. pp. 203–213.

25. Smirnov, A., E. Manakova, and D. Matulis. 2019. Correlations Between Inhibitor Binding Thermodynamics and Co-crystal Structures with Carbonic Anhydrases. In: Matulis D, editor. Carbonic Anhydrase as Drug Target: Thermodynamics and Structure of Inhibitor Binding. Cham: Springer International Publishing. pp. 249–261.

26. Mickevičiūtė, A., V. Juozapaitienė, V. Michailovienė, J. Jachno, J. Matulienė, and D. Matulis. 2019. Recombinant Production of 12 Catalytically Active Human CA Isoforms. In:

Matulis D, editor. Carbonic Anhydrase as Drug Target: Thermodynamics and Structure of Inhibitor Binding. Cham: Springer International Publishing. pp. 15–37.

27. Leitans, J., A. Kazaks, A. Balode, J. Ivanova, R. Zalubovskis, C.T. Supuran, and K. Tars. 2015. Efficient Expression and Crystallization System of Cancer-Associated Carbonic Anhydrase Isoform IX. *J. Med. Chem.* 58:9004–9009.

28. Matulis, D., J.K. Kranz, F.R. Salemme, and M.J. Todd. 2005. Thermodynamic Stability of Carbonic Anhydrase: Measurements of Binding Affinity and Stoichiometry Using ThermoFluor. *Biochemistry*. 44:5258–5266.

29. Petrauskas, V., A. Zubrienė, M.J. Todd, and D. Matulis. 2019. Inhibitor Binding to Carbonic Anhydrases by Fluorescent Thermal Shift Assay. In: Matulis D, editor. Carbonic Anhydrase as Drug Target: Thermodynamics and Structure of Inhibitor Binding. Cham: Springer International Publishing. pp. 63–78.

30. Linkuvienė, V., A. Zubrienė, E. Manakova, V. Petrauskas, L. Baranauskienė, A. Zakšauskas, A. Smirnov, S. Gražulis, J.E. Ladbury, and D. Matulis. 2018. Thermodynamic, kinetic, and structural parameterization of human carbonic anhydrase interactions toward enhanced inhibitor design. *Q. Rev. Biophys.* 51.

31. Koes, D.R., M.P. Baumgartner, and C.J. Camacho. 2013. Lessons Learned in Empirical Scoring with smina from the CSAR 2011 Benchmarking Exercise. *J. Chem. Inf. Model.* 53:1893–1904.

32. Trott, O., and A.J. Olson. 2010. AutoDock Vina: Improving the speed and accuracy of docking with a new scoring function, efficient optimization, and multithreading. *J. Comput. Chem.* 31:455–461.

33. Quiroga, R., and M.A. Villarreal. 2016. Vinardo: A Scoring Function Based on Autodock Vina Improves Scoring, Docking, and Virtual Screening. *PLOS ONE*. 11:e0155183.

34. Santos-Martins, D., S. Forli, M.J. Ramos, and A.J. Olson. 2014. AutoDock4Zn: An Improved AutoDock Force Field for Small-Molecule Docking to Zinc Metalloproteins. *J. Chem. Inf. Model.* 54:2371–2379.

35. Kadukova, M., and S. Grudinin. 2017. Convex-PL: a novel knowledge-based potential for protein-ligand interactions deduced from structural databases using convex optimization. *J Comput Aided Mol Des*. 31:943–958.

36. Waterhouse, A., M. Bertoni, S. Bienert, G. Studer, G. Tauriello, R. Gumienny, F.T. Heer, T.A.P. de Beer, C. Rempfer, L. Bordoli, R. Lepore, and T. Schwede. 2018. SWISS-MODEL: homology modelling of protein structures and complexes. *Nucleic Acids Res*. 46:W296–W303.

37. Kazokaitė, J., V. Kairys, J. Smirnovienė, A. Smirnov, E. Manakova, M. Tolvanen, S. Parkkila, and D. Matulis. 2019. Engineered Carbonic Anhydrase VI-Mimic Enzyme Switched the Structure and Affinities of Inhibitors. *Sci Rep*. 9:12710.

38. Pettersen, E.F., T.D. Goddard, C.C. Huang, G.S. Couch, D.M. Greenblatt, E.C. Meng, and T.E. Ferrin. 2004. UCSF Chimera—A visualization system for exploratory research and analysis. *J. Comput. Chem.* 25:1605–1612.

39. Halgren, T.A. 1999. MMFF VI. MMFF94s option for energy minimization studies. *J. Comput. Chem.* 20:720–729.

40. Hanwell, M.D., D.E. Curtis, D.C. Lonie, T. Vandermeersch, E. Zurek, and G.R. Hutchison. 2012. Avogadro: An advanced semantic chemical editor, visualization, and analysis platform. *J Cheminform*. 4:17.

41. Morris, G.M., R. Huey, W. Lindstrom, M.F. Sanner, R.K. Belew, D.S. Goodsell, and A.J. Olson. 2009. AutoDock4 and AutoDockTools4: Automated docking with selective receptor flexibility. *J. Comput. Chem.* 30:2785–2791.

42. O'Boyle, N.M., M. Banck, C.A. James, C. Morley, T. Vandermeersch, and G.R. Hutchison. 2011. Open Babel: An open chemical toolbox. *J Cheminform*. 3:33.

43. Kabsch, W. 2010. XDS. *Acta Cryst D*. D66:125–132.

44. Battye, T.G.G., L. Kontogiannis, O. Johnson, H.R. Powell, and A.G.W. Leslie. 2011. iMOSFLM: a new graphical interface for diffraction-image processing with MOSFLM. *Acta Cryst. D Biol. Crystallogr.* 67:271–281.

45. Vagin, A., and A. Teplyakov. 2010. Molecular replacement with MOLREP. *Acta Cryst. D Biol. Crystallogr.* 66:22–25.

46. Vagin, A.A., R.A. Steiner, A.A. Lebedev, L. Potterton, S. McNicholas, F. Long, and G.N. Murshudov. 2004. REFMAC5 dictionary: organization of prior chemical knowledge and guidelines for its use. *Acta Crystallogr D Biol Crystallogr*. 60:2184–95.

47. Emsley, P., B. Lohkamp, W.G. Scott, and K. Cowtan. 2010. Features and development of ıt Coot. *Acta Cryst. D*. 66:486–501.

48. Murshudov, G.N., P. Skubák, A.A. Lebedev, N.S. Pannu, R.A. Steiner, R.A. Nicholls, M.D. Winn, F. Long, and A.A. Vagin. 2011. REFMAC5 for the refinement of macromolecular crystal structures. *Acta Cryst. D Biol. Crystallogr.* 67:355–367.

49. Kovalevsky, A., M. Aggarwal, H. Velazquez, M.J. Cuneo, M.P. Blakeley, K.L. Weiss, J.C. Smith, S.Z. Fisher, and R. McKenna. 2018. "To Be or Not to Be" Protonated: Atomic Details of Human Carbonic Anhydrase-Clinical Drug Complexes by Neutron Crystallography and Simulation. *Structure*. 26:383-390.e3.

50. Koruza, K., B.P. Mahon, M.P. Blakeley, A. Ostermann, T.E. Schrader, R. McKenna, W. Knecht, and S.Z. Fisher. 2019. Using neutron crystallography to elucidate the basis of selective inhibition of carbonic anhydrase by saccharin and a derivative. *J. Struct. Biol.*

51. Fisher, S.Z., M. Aggarwal, A.Y. Kovalevsky, D.N. Silverman, and R. McKenna. 2012. Neutron Diffraction of Acetazolamide-Bound Human Carbonic Anhydrase II Reveals Atomic Details of Drug Binding. *J. Am. Chem. Soc.* 134:14726–14729.

52. Smirnov, A., A. Zubrienė, E. Manakova, S. Gražulis, and D. Matulis. 2018. Crystal structure correlations with the intrinsic thermodynamics of human carbonic anhydrase inhibitor binding. *PeerJ*. 6:e4412.

53. Ma, H., A. Li, and K. Gao. 2017. Network of Conformational Transitions Revealed by Molecular Dynamics Simulations of the Carbonic Anhydrase II Apo-Enzyme. *ACS Omega*. 2:8414–8420.

54. Ashton, M.J., D.C. Cook, G. Fenton, J.-A. Karlsson, M.N. Palfreyman, D. Raeburn, A.J. Ratcliffe, J.E. Souness, S. Thurairatnam, and N. Vicker. 1994. Selective Type IV Phosphodiesterase Inhibitors as Antiasthmatic Agents. The Syntheses and Biological Activities of 3-(Cyclopentyloxy)-4-methoxybenzamides and Analogs. *J. Med. Chem.* 37:1696–1703.

55. Ilies, M.A., B. Masereel, S. Rolin, A. Scozzafava, G. Câmpeanu, V. Cîmpeanu, and C.T. Supuran. 2004. Carbonic anhydrase inhibitors: aromatic and heterocyclic sulfonamides incorporating adamantyl moieties with strong anticonvulsant activity. *Bioorg Med Chem*. 12:2717–2726.

Cover art